3134–3142 *Nucleic Acids Research, 2009, Vol. 37, No. 10* *Published online 11 March 2009*
doi:10.1093/nar/gkp119

A recurrent magnesium-binding motif provides a framework for the ribosomal peptidyl transferase center

Chiaolong Hsiao and Loren Dean Williams*

School of Chemistry and Biochemistry, Parker H. Petit Institute of Bioengineering and Bioscience, Georgia Institute of Technology, Atlanta, *GA* 30332-0400, USA

Received October 23, 2008; Revised February 7, 2009; Accepted February 11, 2009

ABSTRACT

The ribosome is an ancient macromolecular machine responsible for the synthesis of all proteins in all living organisms. Here we demonstrate that the ribosomal peptidyl transferase center (PTC) is supported by a framework of magnesium microclusters (Mg^{2+}-μc's). Common features of Mg^{2+}-μc's include two paired Mg^{2+} ions that are chelated by a common bridging phosphate group in the form $Mg^{2+}_{(a)}$–(O1P-P-O2P)–$Mg^{2+}_{(b)}$. This bridging phosphate is part of a 10-membered chelation ring in the form $Mg^{2+}_{(a)}$–(OP-P-O5′-C5′-C4′-C3′-O3′-P-OP)–$Mg^{2+}_{(a)}$. The two phosphate groups of this 10-membered ring are contributed by adjacent residues along the RNA backbone. Both Mg^{2+} ions are octahedrally coordinated, but are substantially dehydrated by interactions with additional RNA phosphate groups. The Mg^{2+}-μc's in the LSU (large subunit) appear to be highly conserved over evolution, since they are unchanged in bacteria (*Thermus thermophilus*, PDB entry 2J01) and archaea (*Haloarcula marismortui*, PDB entry 1JJ2). The 2D elements of the 23S rRNA that are linked by Mg^{2+}-μc's are conserved between the rRNAs of bacteria, archaea and eukarya and in mitochondrial rRNA, and in a proposed minimal 23S-rRNA. We observe Mg^{2+}-μc's in other rRNAs including the bacterial 16S rRNA, and the P4–P6 domain of the tetrahymena Group I intron ribozyme. It appears that Mg^{2+}-μc's are a primeval motif, with pivotal roles in RNA folding, function and evolution.

INTRODUCTION

Recent structures of large RNAs, such as the P4–P6 domain of the tetrahymena ribozyme (1–5), and larger RNAs such as ribosomes (6–14) continue to reveal important new principles of RNA structure and folding. Globular cores of large RNAs are characterized by base–base tertiary interactions and 'buried' phosphate groups (15,16). During RNA-folding cations are sequestered from bulk solvent, and held in close proximity to the polymer. Folding increases proximities of phosphate groups, and the electrostatic repulsion among them. Thus phosphate–phosphate repulsion must be offset by attraction between phosphates and cations.

Mg^{2+}, since the beginning of life, has been closely associated with some of the central players in biological systems—phosphates and phosphate esters (17). Mg^{2+} shares a special geometric, electrostatic, thermodynamic relationship with phosphates (18). The ionic radius of Mg^{2+} is small (0.65 Å), the charge density is high, the coordination geometry is octahedral (the AOCN—average observed coordination number—is 5.98), the preferred ligands are charged or neutral oxygens, and the hydration enthalpy is large (−458 kcal/mol) (19–22). Ligand–ligand crowding is one of the hallmarks of Mg^{2+} complexes, leading to highly restrained ligand–Mg^{2+}–ligand geometry, and strong ligand–ligand repulsive forces. In comparison with group I ions, Ca^{2+} or polyamines, Mg^{2+} has a much greater affinity for phosphate oxygens, and binds to them with well-defined geometry. Unlike other cations, Mg^{2+} brings phosphate oxygens in its first shell into direct contact with each other.

Chelation effects and topology influence interactions of nucleic acids with ions. For example magnesium forms a *mononuclear* motif with ADP/ATP in which one Mg^{2+} ion is chelated by a six-membered ring consisting of atoms $Mg^{2+}_{(a)}$–O^{α}P-P-O-P-O^{β}P–$Mg^{2+}_{(a)}$ (18). Here we observe that a framework of *dinuclear* magnesium complexes $Mg^{2+}_{(a)}$–RNA–$Mg^{2+}_{(b)}$ flanks the peptidyl transferase center (PTC) in LSU ribosomal structures (Figure 1). In these dinuclear clusters, two Mg^{2+} ions are chelated by a common bridging phosphate group. Additional

*To whom correspondence should be addressed. Tel: +1 404 894 9752; Fax: +1 404 894 7452; Email: loren.williams@chemistry.gatech.edu

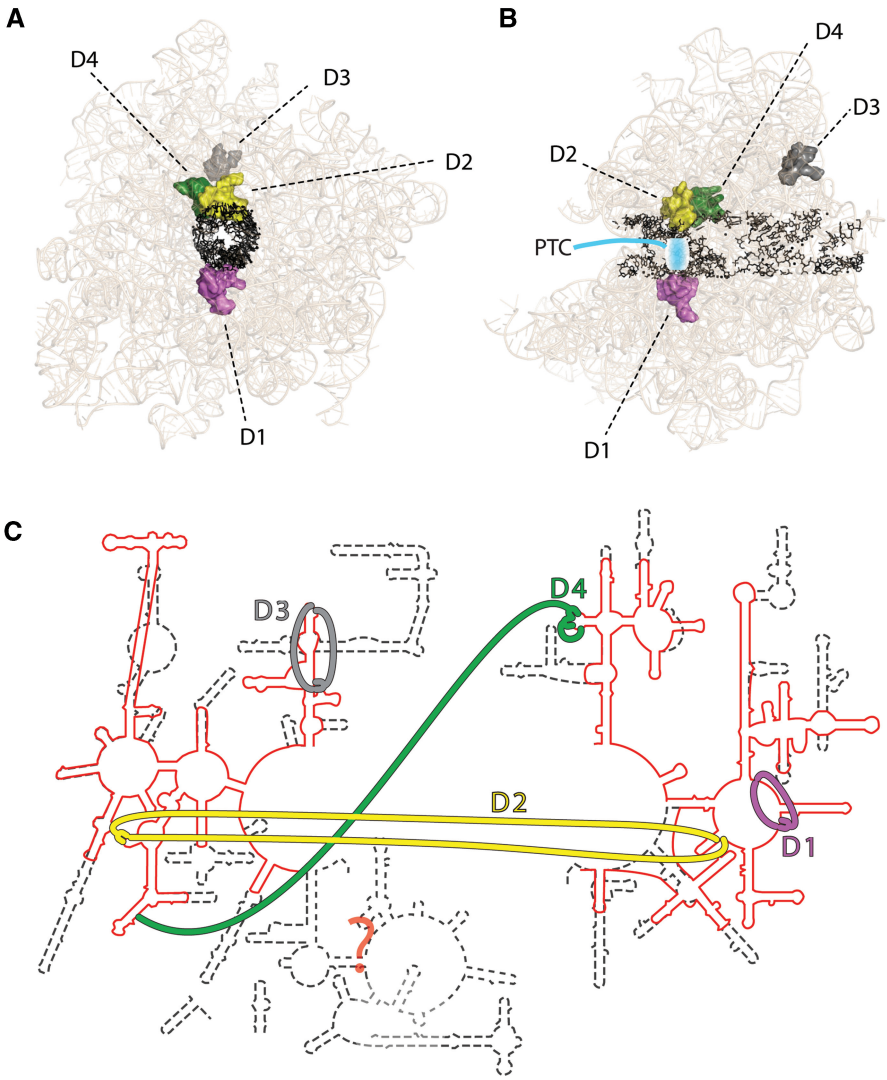

Figure 1. Four Mg^{2+}-μc's are observed in the LSU of *H. marismortui* (PDB entry 1JJ2). (**A**) View into the Peptidyl Transfer Center. The four Mg^{2+}-μc's are represented as solid surfaces. The RNA atoms lining the polypeptide exit tunnel are accented in black. Mg^{2+}-μc's D1, D2 and D4 encircle the PTC. Mg^{2+}-μc's are colored: D1, purple; D2, yellow; D3, gray; D4, green. Ribosomal proteins and the 5S rRNA are omitted for clarity. (**B**) This view, looking across the polypeptide exit tunnel, is rotated by 90° relative to that of panel A. (**C**) The secondary structures of LSU rRNAs of *H. marismortui* [23S rRNA (7), dashed black line] and the mitochondrion of *B. taurus* [16S rRNA (51), red line]. Phosphate groups that are linked by magnesium ions within Mg^{2+}-μc's are indicated by broad colored lines. The secondary structural elements that interact with Mg^{2+}-μc's are conserved in these widely divergent LSUs. In the *C. elegans* LSU (not shown), the rRNA that binds to D3 is absent (52). The question mark indicates the portion of the mitochondrial *B. Taurus* LSU rRNA for which the secondary structure is unknown.

structural features are conserved among these clusters, which are also identified in other RNAs, indicating that *dinuclear* RNA magnesium clusters compose by distinctive yet recurrent motif. This dinuclear $Mg^{2+}_{(a)}$–RNA–$Mg^{2+}_{(b)}$ motif is referred to here as the magnesium microcluster (Mg^{2+}-μc).

MATERIALS AND METHODS

Molecular interactions

Ribosomal and other RNA structures were obtained from the PDB (23) and subject to automated (24–28) and manual structural analysis and decomposition. Because its resolution is greatest, the *Haloarcula marismortui* LSU is used as the benchmark and the basis for comparison. First, shell Mg^{2+}–ligand interactions are defined by distances less than 2.4 Å (18). The Mg^{2+} positions in 23S-rRNA^{HM} are, as determined by various geometric criteria, highly credible, with a few exceptions. The Mg^{2+} to oxygen distance is an excellent metric in that the predicted and observed (in 23S-rRNA^{HM}) frequencies reach distinct maxima at 2.1 Å and fall to nearly zero by 2.6 Å. The thermal factors of the Mg^{2+} atoms in the Mg clusters do not suggest partial occupancy (i.e. they are not in general significantly higher than nearby atoms.) As indicated by relative OP (phosphate oxygen atom) positions, essentially all relevant Mg^{2+} ions were added correctly to

the 1JJ2 model. An exhaustive survey of all Mg^{2+}–RNA interactions in the database was conducted with the MeRNA database (29). Hydrogen bond distances are defined by distances less than 3.4 Å between hydrogen bond donating and accepting heavy atoms.

Sequence homology and alignment

The fragment of ribosomal protein L2 that associates with the *H. marismortui* D2 complex (PNVRGVAMNA VDHPFGGG, peptide L2/D2) was determined by inspection of the 3D structure (1JJ2). That sequence was used as a search string in Blast (30), finding matches in all cytoplasmic and chloroplast ribosomes and in fungal mitoribosomes, but not in other mitoribosomes or in other chloroplast ribosomes. Exhaustive searching failed to find L2/D2 homologs in nonfungal mitoribosomes. Protein alignment was performed with Clustalw (31).

Structural alignment

To date, structural alignment of very large RNAs remains challenge due to the large size, intricate backbone choreography and tertiary interactions. We developed a heuristic method, using a '*Divide and Conquer*' strategy for performing whole body superimposition of 23s rRNAs. With this method (to be described elsewhere), the alignment and superimposition of the 23s rRNAs of *Thermus thermophilus* and *H. marismortui* gives an overall RMSD of atomic positions of 1.2 Å. This superimposition utilizes 73% of RNA backbone atoms (around 2129 residues). This accurate superimposition allows one to identify conserved Mg^{2+} ions.

RESULTS

Forty-one Mg^{2+} ions in *H. marismortui* LSU were determined by geometric analysis to be highly coordinated by rRNA phosphate groups [more than one phosphate group in the Mg^{2+} first shell, also see (11)]. Visual inspection of each of these Mg^{2+} ions revealed that four pairs are distinctive environments, leading to our classification of them as Mg^{2+}-μc's.

The basic motif of the Mg^{2+}-μc is defined by several features (Figure 2A). Two paired Mg^{2+} ions are chelated by a common bridging phosphate group in the form $Mg^{2+}_{(a)}$–(O1P-P-O2P)–$Mg^{2+}_{(b)}$. This bridging phosphate is part of a 10-membered chelation ring in the form $Mg^{2+}_{(a)}$–(OP-P-O5′-C5′-C4′-C3′-O3′-P-OP)–$Mg^{2+}_{(a)}$. The two phosphate groups of this 10-membered ring are contributed by adjacent residues along the RNA backbone. Both Mg^{2+} ions are octahedrally coordinated, but are substantially dehydrated by interactions with additional RNA phosphate groups.

The conformation of the RNA and the positions of the Mg^{2+} ions are substantially conserved in a Mg^{2+}-μc. The position and conformation of the RNA is constrained by the Mg^{2+} ions. The relative positions of the Mg^{2+} ions are constrained by the $Mg^{2+}_{(a)}$–(O1P-P-O2P)–$Mg^{2+}_{(b)}$ bridges. The superimposition of four Mg^{2+}-μc's is shown in Figure 2B. The RMSD of the atomic positions of this superimposition is 0.59 Å.

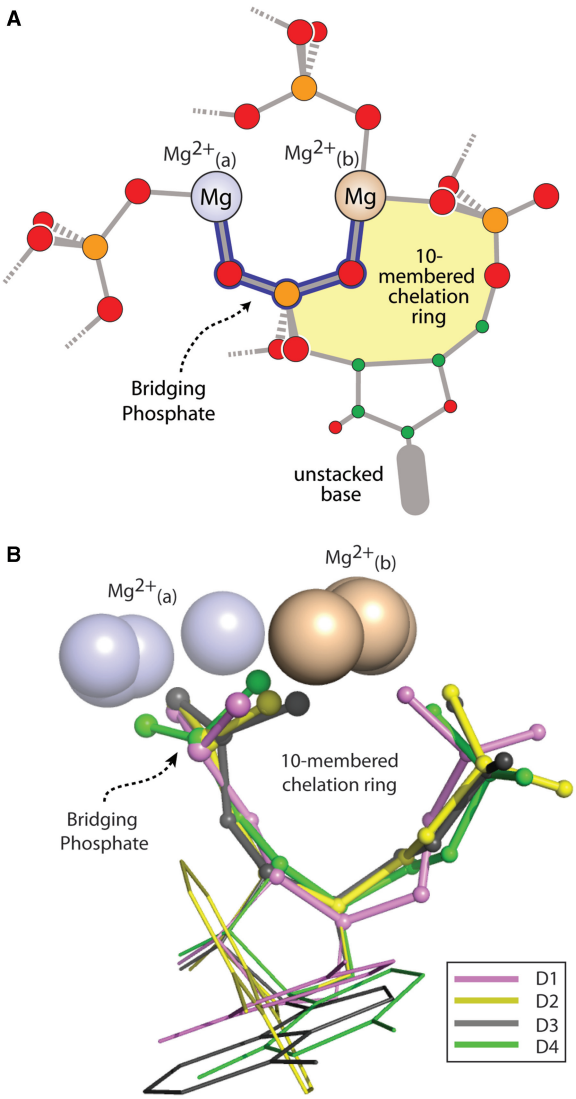

Figure 2. The Mg^{2+}-μc motif. (**A**) A schematic diagram illustrating the $Mg^{2+}_{(a)}$–(O1P-P-O2P)–$Mg^{2+}_{(b)}$ bridge (outlined in blue), the 10-membered chelation ring (yellow), an unstacked base and the additional RNA phosphate groups that enter the Mg^{2+} first shell at variable positions. Carbon is green, oxygen is red and phosphorous is orange. Magnesium (a) is cyan while magnesium (b) is brown. (**B**) Superimposition of four Mg^{2+}-μc's (D1 purple, D2 yellow, D3 gray and D4 green) from the *H. marismortui* LSU. All of the atoms shown here were used in the superimposition of the clusters except for the RNA bases.

Although the basic motif is conserved in all four clusters, Mg^{2+}-μc's are elaborated by additional RNA ligands. RNA phosphate groups that are not part of the bridging phosphate or the 10-membered ring can enter the Mg^{2+} coordination sphere at various positions. Each Mg^{2+}-μc is defined *in toto* by two paired Mg^{2+} ions plus all RNA residues that engage in first shell interactions with the paired Mg^{2+} ions. Therefore each Mg^{2+}-μc has a unique shape. Specific descriptions of the four clusters are provided here.

Mg^{2+}-μc D2

In this cluster, the $Mg^{2+}_{(a)}$–(O1P-P-O2P)–$Mg^{2+}_{(b)}$ bridge is composed of the phosphate group of G877 along with Mg^{2+} ions 8003 and 8013 (Figure 3A). The 10-membered $Mg^{2+}_{(a)}$–(OP-P-O5′-C5′-C4′-C3′-O3′-P-OP)–$Mg^{2+}_{(a)}$ system is composed of the phosphate group and ribose atoms of A876 along with the phosphate group of G877. Both phosphates from that segment of RNA chelate Mg^{2+} 8003.

The two Mg^{2+} ions 8003 and 8013 of Mg^{2+}-μc D2 jointly link RNA segments that are remote in the linear sequence and in the secondary structure (32). These linkages take the form of first shell $OP_{(i)}$–Mg^{2+}-$OP_{(j)}$, where $j >> i$. Mg^{2+} 8003 links the phosphates of A876 and G877 to the phosphate of A2624. Mg^{2+} 8013 links the phosphate of G877 to the phosphate of G2623. The Mg^{2+}-μc D2 linkages are indicated by the long yellow strips in the secondary structure in Figure 1C.

The first shell RNA–Mg^{2+} interactions unstack the bases (Figure 3A, bottom panel). Residue A876 is unstacked from G877, with a C1′–C1′ distance (A876 to G877) of 7.2 Å. Residue A2622 is unstacked from G2623 ($r_{C1'-C1'}$ = 7.4 Å). This unstacking is important for assembly. The unstacked face of G877 forms part of the cavity for protein L2 (below). A2622 (unstacked in Mg^{2+}-μc D2) intercalates between U1838 and A1839 (Mg^{2+}-μc D4, below).

Mg^{2+}-μc D4

In this cluster the $Mg^{2+}_{(a)}$–(O1P-P-O2P)–$Mg^{2+}_{(b)}$ bridge is composed of the phosphate group of U1839 along with Mg^{2+} ions 8005 and 8007 (Figure 3B). There are two 10-membered ring systems. One $Mg^{2+}_{(a)}$–(OP-P-O5′-C5′-C4′-C3′-O3′-P-OP)–$Mg^{2+}_{(a)}$ system is composed of the phosphate group and ribose atoms of U1838 plus the phosphate group of A1839, along with Mg^{2+} 8005, which is also chelated by the phosphate of A1836. A second $Mg^{2+}_{(a)}$–(OP-P-O5′-C5′-C4′-C3′-O3′-P-OP)–$Mg^{2+}_{(a)}$ system is composed of the phosphate group and ribose atoms of A1839 along plus the phosphate group of A1840. This RNA segment chelates Mg^{2+} 8007.

These Mg^{2+}–RNA interactions induce an extended array of unstacked bases (Figure 3B, bottom panel). Residue U1835 is unstacked from A1836 ($r_{C1'-C1'}$ = 9.6 Å). Residue A1836 is unstacked from G1837 ($r_{C1'-C1'}$ = 6.6 Å). Residue G1837 is unstacked from U1838 ($r_{C1'-C1'}$ = 8.8 Å). Residue U1838 is unstacked from A1839 ($r_{C1'-C1'}$ = 7.7). Residue A1839 is unstacked from A1840 ($r_{C1'-C1'}$ = 7.8 Å). These unstacked bases of Mg^{2+}-μc D4 provide a complementary docking surface for Mg^{2+}-μc D2 (Figure 4). As noted above A2622 (of Mg^{2+}-μc D2) intercalates between U1838 and A1839 (of Mg^{2+}-μc D4).

Mg^{2+} ion 8007 of Mg^{2+}-μc D4 links RNA segments that are remote in the linear sequence and in the secondary structure. This Mg^{2+} ion links the phosphates of A1839 and A1840 and to the phosphate of U832. This linkage is indicated by the long green strip in the secondary structure in Figure 1C.

Mg^{2+}-μc D1

This cluster has a double bridge. One $Mg^{2+}_{(a)}$–(O1P-P-O2P)–$Mg^{2+}_{(b)}$ bridge is composed of the phosphate group of C2534 along with Mg^{2+} ions 8001 and 8002 (Figure 3C). A second $Mg^{2+}_{(a)}$–(O1P-P-O2P)–$Mg^{2+}_{(b)}$ linkage is composed of the phosphate group of A2483, which joins the same two Mg^{2+} ions. The double bridge is associated with a decreased Mg^{2+}–Mg^{2+} distance, as illustrated by the shift of one Mg^{2+} relative to its homologs in Figure 2B. The 10-membered $Mg^{2+}_{(a)}$–(OP-P-O5′-C5′-C4′-C3′-O3′-P-OP)–$Mg^{2+}_{(a)}$ system is composed of the phosphate group and ribose atoms of C2533 along with the phosphate group of C2534. This segment of RNA chelates Mg^{2+} 8001.

Both Mg^{2+} ions link RNA segments that are not adjacent in the linear sequence or secondary structure. The OPs of A2483 are linked to the phosphates of C2533 (one OP) and C2534 (both OPs) in a joint interaction involving both Mg^{2+} ions. These RNA–Mg^{2+} interactions unstack G2482 from A2483 (Figure 3C, bottom panel; $r_{C1'-C1'}$ = 8.3 Å). In addition, A2532 is unstacked from C2533 ($r_{C1'-C1'}$ = 6.9 Å).

Mg^{2+}-μc D3

The $Mg^{2+}_{(a)}$–(O1P-P-O2P)–$Mg^{2+}_{(b)}$ bridge in this cluster is composed of the phosphate group of C1679 along with Mg^{2+} ions 8016 and 8029 (Figure 3D). The 10-membered $Mg^{2+}_{(a)}$–(OP-P-O5′-C5′-C4′-C3′-O3′-P-OP)–$Mg^{2+}_{(a)}$ system is composed of the phosphate group and ribose atoms of A1678 along with the phosphate group of C1679. This segment of RNA chelates Mg^{2+} 8016.

Both Mg^{2+} ions link RNA segments that are not adjacent in the linear sequence or secondary structure. An OP of A1678 and an OP of C1679 are linked by Mg^{2+} 8016 to an OP of A1504. An OP of C1679 is linked via Mg^{2+} 8029 to an OP of U1503. These RNA–Mg^{2+} interactions unstack the bases (Figure 3D, bottom panel). U1677 is unstacked from A 1678 ($r_{C1'-C1'}$ = 8.0 Å). Residue A1502 is unstacked from U1503 ($r_{C1'-C1'}$ = 7.7)

Role of Mg^{2+}-μc's in activity

Three Mg^{2+}-μc's (D1, D2 and D4) flank the PTC. These Mg^{2+}-μc's are not directly involved in catalysis, and do not form the innermost layer of the PTC, but provide the framework and supporting structure for RNA that does. Mg^{2+}-μc's lend critical support to function by forming convoluted binding surfaces and providing rigid frameworks for attachment and buttressing of catalytic residues.

The fourth cluster (D3) is located near the exit site of the polypeptide exit tunnel. Previously Steitz and Moore (11,32) showed that within the LSU, the concentration of Mg^{2+} ions is greatest near PTC. They also described one 'magnesium cluster' (part of Mg^{2+}-μc D2).

Mg^{2+}-μc—ribosomal protein interactions

Mg^{2+}-μc D2 is associated with ribosomal protein L2. Inspection of the structures reveal an 18 amino-acid loop of L2 (loop-L2/D2, Table 1) forms a binding

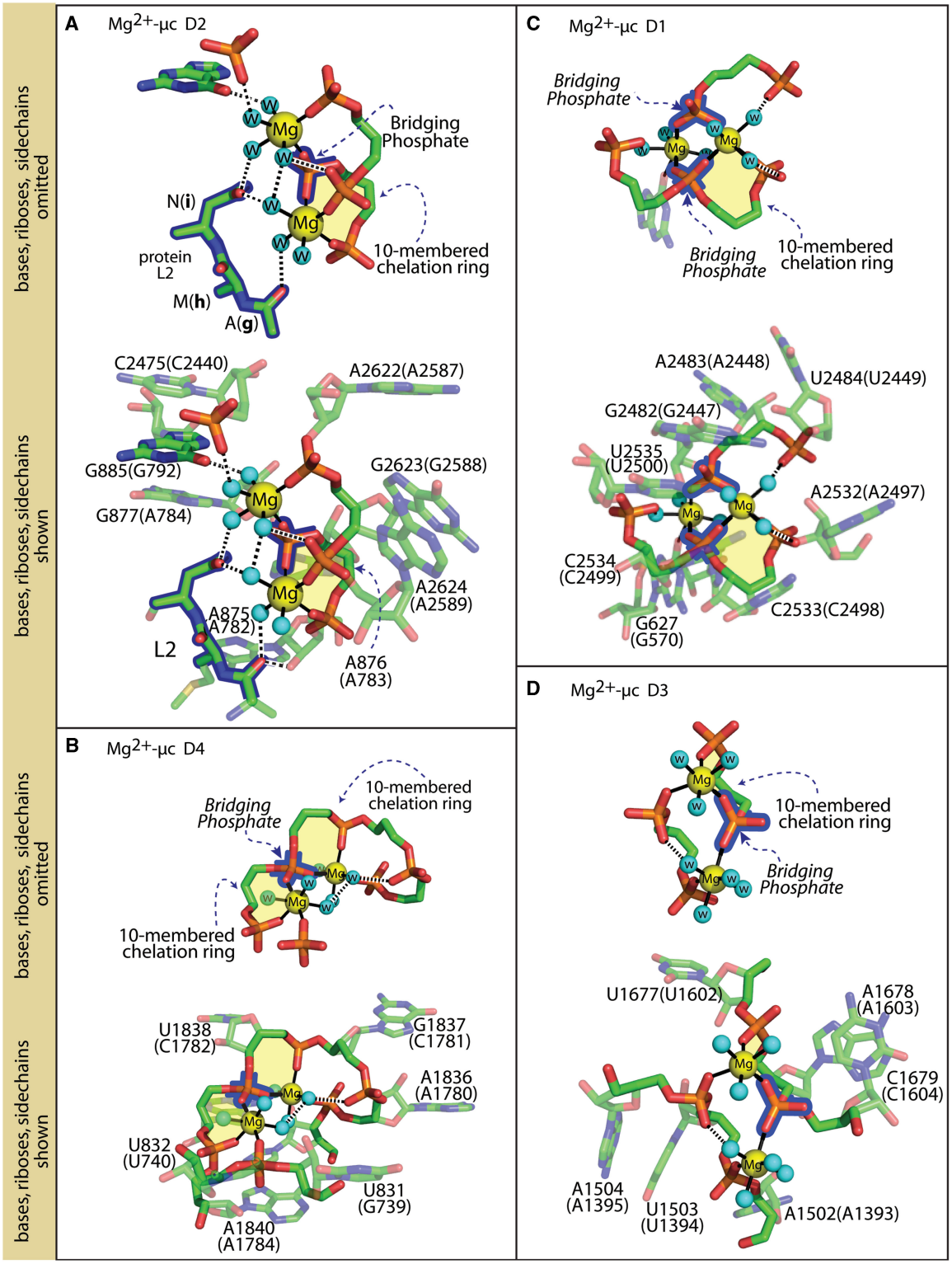

Figure 3. Atomic level representations of the four Mg^{2+}-μc's of *H. marismortu* LSU (PDB entry 1JJ2). The bridging phosphates group are outlined in blue and the 10-membered chelation rings are shaded in yellow. (**A**) Top: Mg^{2+}-μc D2 with bases, riboses (except C3′, C4′, C5′) and protein sidechains omitted (Mg^{2+} ions 8003 and 8013). A three residue fragment of ribosomal protein L2 contains universally conserved asparagine (i) and methione (h). Bottom: Mg^{2+}-μc D2 with bases, riboses and protein sidechains included. (**B**) Top: Mg^{2+}-μc D4 with bases and riboses omitted (Mg^{2+} ions 8005 and 8007). This Mg^{2+}-μc has two 10-membered chelation rings. Bottom: Bases and riboses are included. (**C**) Top: Bases and riboses omitted (Mg^{2+} ions 8001 and 8002). This Mg^{2+}-μc has two $Mg^{2+}_{(a)}$-O1P-P-O2P-$Mg^{2+}_{(b)}$ bridges (phosphates of residues C2534 and A2483). Bottom: Bases and riboses are included. (**D**) Top: Mg^{2+}-μc D3 with bases and riboses omitted (Mg^{2+} ions 8016 and 8029). Bottom: Bases and riboses are included. First-shell Mg^{2+} contacts are black solid lines. Hydrogen bonds are dashed lines. Carbon is green, oxygen is red, phosphorous is orange and magnesium is yellow. Residue labels in parentheses are from *T. Thermophilus*, using the *E. coli* numbering scheme.

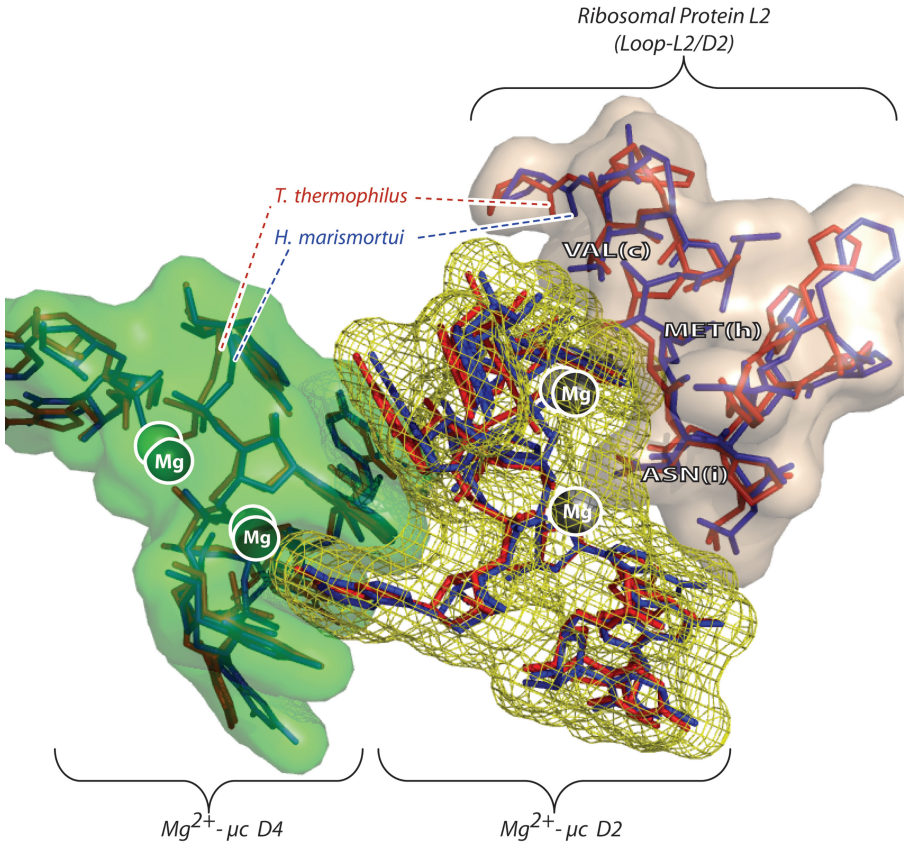

Figure 4. The complex formed by Mg^{2+}-μc's D4 and D2 and the loop-L2/D2 of ribosomal protein L2. Structures of both *H. marismortui* and *T. Thermophilus* are shown. Magnesium ions are indicated by spheres. When the 23S rRNAs of *H. marismortui* and *T. thermophilus* are superimposed using 73% of rRNA backbone atoms, the RMSD of atomic positions of the eight Mg^{2+} ions within the four Mg^{2+}-μc's is very small, only 0.4 Å.

Table 1. Mg^{2+}-μc D2-binding loop of ribosomal protein L2 (loop-L2/D2)[a]

Species	Code	Amino-acid sequence[b] NNNNNNNNNNNNNNNNabcdefghijklmnopqrNNNN[c]
Homo sapiens	EAW82048.1	KAGRAYHKYKAKRNCW**P**R**V**R**G**V**A**M**N**P**V**E**H**P**F**G**G**G**-NHQ
Caenorhabditis elegans	NP_507940.1	KAGRSYHKYKAKRNSW**P**R**V**R**G**V**A**M**N**P**V**E**H**P**H**G**G**G**-NHQ
Saccharomyces cerevisiae	P05736.3	KAGRAFHKYRLKRNSW**P**K**T**R**G**V**A**M**N**P**V**D**H**P**H**G**G**G**-NHQ
Haloarcula marismortui[d]	AAA86862.1	KAGNKHHKMKARGTKW**P**N**V**R**G**V**A**M**N**A**V**D**H**P**F**G**G**G**-GRQ
Escherichia coli	BAE77974.1	KAGAARWRGVR- - - -**P**T**V**R**G**T**A**M**N**P**V**D**H**P**H**G**G**G**EGRN
Thermus thermophilus[e]	AAS81667.1	KAGRSRWLGRR- - - -**P**H**V**R**G**A**A**M**N**P**V**D**H**P**H**G**G**G**EGRA
Arabidopsis thaliana-chloro[f]	NP_051123.1	RAGSKCWLGKR- - - -**P**V**V**R**G**V**V**M**N**P**V**D**H**P**H**G**G**G**EGRA
Saccharomyces cerevisiae-mito[f]	NP_010864.1	KAGRSRWLGIR- - - -**P**T**V**R**G**V**A**M**N**K**C**D**H**P**H**G**G**G**RGKS
Homo sapiens-mito[g]	NP_057034.2	KAGRNRWLGKR- - - -*PNSGRWHRKGGWAGRKIRPLPP*

[a]The eukaryotic equivalent of ribosomal protein L2 is L8. The mitochondrial equivalent of L2 is rml2. Blue text indicates conserved sequences in all ribosomes including mitoribosomes. Red text indicates conserved sequences in all cytoplasmic and chloroplast ribosomes and in fungal mitoribosomes, but not in other mitoribosomes. The ordering of this table was obtained from the complete L2/L8/rml2 sequence alignment with ClustalW (31).
[b]Loop-L2/D2 is bold. Observed sequence changes of loop-L2/D2 are conservative.
[c]Positions of loop-L2/D2 are defined by amino acid positions a–r.
[d]Loop-L2/D2 contains ribosomal protein L2 residues 187–204 in *H. marismortui*.
[e]Loop-L2/D2 contains ribosomal protein L2 residues 219–226 in *T. thermophilus*.
[f]Loop-L2/D2 contains ribosomal protein rml2 residues 331–348 in *S. cerevisiae*. Mitochondrial and chloroplast ribosomes are thought to have undergone major remodeling (51,53,54) and are the most divergent from other ribosomes.
[g]The *H. sapiens* mitoribosome lacks loop-L2/D2 as do other non-fungal mitoribosomes.

pocket for Mg^{2+}-μc D2. As shown in Figures 3A and 4, methionine (h) and valine (c) along with the backbone carbonyl of an alanine (g) form a cleft for A875 ($A782^{TT}$). Asparagine (i) and the carbonyl oxygen of alanine (g) bind to the first shell water molecules of the Mg^{2+} ions. Histidine (m) forms part of the tightly packed core of loop-L2/D2 (data not shown). The conformation of loop L2/D2 is highly conserved between *T. thermophilus* and *H. marismortui* (Figure 4). The RMSD of atomic positions of loop-L2/D2 is 0.6 Å in the globally

superimposed LSUs (*H. marismortui* versus *T. thermophilus*, using all atoms of 18 residues except for differing sidechains for the RMSD calculation, 110 atoms total).

Mg^{2+}-μc's in other RNAs

As shown in the Supplementary Data, Mg^{2+}-μc's are observed not only in the 23S rRNA, but also in the bacterial 16S rRNA (8), the P4–P6 domain of the tetrahymena Group I intron ribozyme (2). A related magnesium cluster is found in Group II intron ribozyme (33).

DISCUSSION

Mg^{2+}-μc structure

Four Mg^{2+}-μc's (Microclusters D1, D2, D3 and D4; Figure 1) are found within the LSU of *H. marismortui* [an archaebacterium, PDB entry 1JJ2 (7)]. These four Mg^{2+}-μc's are also found within the LSU of *T. thermophilus* [a bacterium, PDB entry 2J01 (13)]. The Mg^{2+}-μc's are highly conserved in position, conformation and interactions between the two LSUs. Mg^{2+}-μc's are defined by common features (Figure 2A) including (i) chelation of two Mg^{2+} ions by a common bridging phosphate in the form of $Mg^{2+}_{(a)}$–(O1P-P-O2P)–$Mg^{2+}_{(b)}$, (ii) chelation of one of these Mg^{2+} ions by phosphate groups of adjacent residues in the form of $Mg^{2+}_{(a)}$–(OP-P-O5′-C5′-C4′-C3′-O3′-P-OP)–$Mg^{2+}_{(a)}$, (iii) unpaired and unstacked bases with non-canonical RNA conformations and (iv) and close proximity to regions of function.

Mg^{2+}-μc's are unique structural entities with rigidity and forced dispositions of functional groups that would be difficult to achieve by RNA alone or by RNA in association with group 1 cations. Mg^{2+}-μc's by nature of their $Mg^{2+}_{(a)}$–(O1P-P-O2P)–$Mg^{2+}_{(b)}$ linkages impose unusual constraints on RNA conformation and force unstacking of bases. The bridging phosphate is, like all phosphates, restricted to tetrahedral geometry. The ligands of Mg^{2+} ions are restricted to octahedral geometry. Mg^{2+}-μc is composed of two octahedra linked by a tetrahedral phosphorous atom. Therefore, the core of each cluster is geometrically rigid and tightly packed. In addition, it can be seen that the RNA of Mg^{2+}-μc's form intricate and convoluted surfaces (Figure 4), in part facilitating their association with other RNA and with protein.

Ordinarily, the conformational space accessible to RNA is rather limited, and is driven by stacking interactions and double-strand formation. Noller (34) has suggested that small molecules can extend the repertoire of RNA structure, and may have performed that role during early evolution. Magnesium, like a small molecule, can drive RNA into unusual conformation states (11,18). Mg^{2+}-μc's demonstrate not only Mg^{2+}-driven deviation from canonical stacked conformations, but show how these altered states increase surface undulation, and facilitate highly specific interactions, such as those between Mg^{2+}-μc D2 and Mg^{2+}-μc D4 and those between Mg^{2+}-μc D2 and loop-L2/D2 of ribosomal protein L2 (Figure 4).

RNA–protein interactions

Mg^{2+}-μc D2 is associated with ribosomal protein L2 in the LSU. Mutations in ribosomal protein L2 degrade ribosome activity (35–38). The amino-acid sequence of the N-terminal region of ribosomal protein L2 appears to be among the most highly conserved in the phylogenic tree (Table 1). An 18 amino-acid loop of L2 (loop-L2/D2) forms a binding pocket for Mg^{2+}-μc D2. Ten amino-acid residues of loop-L2/D2 are universally conserved in all cytoplasmic and chloroplast ribosomes and in fungal mitoribosomes. Mutations of other residues of loop-L2/D2 are infrequent and are between analogous amino acids such as aspartic acid and glutamic acid or between valine and threonine.

Prior to the availability of ribosome structures in 2000, a direct role for rL2 in catalysis appeared to be consistent with phylogenic, mutagenesis and biochemical data. But a catalytic role for L2 is ruled out by the realization that the ribosome is a ribozyme (10,39,40). The strict sequence conservation of loop-L2/D2 appears to arise from a requirement for complementarily of the L2 protein surface with that of Mg^{2+}-μc D2 (Figures 3A and 4). Because its mutation knocks out PTC activity, His(m) (i.e. histidine residue m of loop L2/D2, Table 1) was previously thought to be part of a serine-protease like charge-relay system. It now appears that the importance of His(m) arises from stabilization of loop-L2/D2 in the appropriate conformation for association with Mg^{2+}-μc D2. The conformation of loop L2/D2 is highly conserved between *T. thermophilus* and *H. marismortui* (Figure 4).

Microclusters in other RNAs

Mg^{2+}-μc's are observed in other ribozymes. A Mg^{2+}-μc, shown in the Supplementary Data, is observed in the P4–P6 domain of the tetrahymena Group I intron ribozyme (2). A Mg^{2+}-μc in the 16S rRNA of *T. thermophilus* [PDB entry 1FJG (41)], appears to be disrupted upon ribosomal assembly [PDB entry 2J00 (13)]. The SARS s2m RNA described by Scott contains a pair of Mg^{2+} ions linked by a single phosphate (42), but those Mg^{2+} are otherwise fully hydrated, with no additional RNA ligands and so do not constitute a Mg^{2+}-μc.

Reasonable coordination geometry in a Mg^{2+}-μc results in Mg^{2+}-Mg^{2+} distances of 5.3–5.6 Å (except for the doubly bridged D1 cluster, with a Mg^{2+}–Mg^{2+} distance of 4.7 Å). Mg^{2+}-μc's differ from the Mg^{2+} complexes proposed in the two-Mg^{2+} catalyzed phosphoryl-transfer mechanism (43,44). In those complexes, a phosphate oxygen (not a phosphate group) bridges two Mg^{2+} ions, with a Mg^{2+}–Mg^{2+} distance of 3.9 Å.

Evolution

Our discussion here makes use of the basic elements of the comparative approach (45) where history is reconstructed by degree of similarity between homologous structures or sequences. Biologists have long used macroscopic structure (skeletal, cellular, etc.) to infer phylogenetic relationships. The logic of that approach extends to the level of macromolecular structure. Comparison between

homologous macromolecular structures can provide information on very distant evolutionary events, because macromolecular structure changes more slowly than sequence over evolutionary time (46,47).

The Mg^{2+}-μc's in the LSU appear to be highly conserved over evolution, since they are unchanged in bacteria (*T. thermophilus*) and archaea (*H. marismortui*), which are thought to have diverged at the LUCA, several billions of years ago (48). Mg^{2+}-μc's are found in association with the most conserved rRNA secondary structures (Figure 1C). Mg^{2+}-μc's link these conserved secondary structural elements via 'electrostatic tertiary interactions', which are composed of phosphate-Mg^{2+}-phosphate interactions. As shown in Figure 1C, the 2D elements of the 23S rRNA that are linked by Mg^{2+}-μc's are conserved between the rRNAs of bacteria, archaea and eukarya (49) and the LSU rRNA of mitochondria (50,51), and in a proposed minimal LSU rRNA (52). The exception is Mg^{2+}-μc D3, which has been dispensed of in some mitoribosomes (such as that of *Caenorhabditis elegans)* by conversion of the RNA-based polypeptide exit tunnel to a protein-based tunnel (51).

We suggest that Mg^{2+}-μc's represent a primeval motif, with roles in RNA folding and catalysis that have found utility over deep evolutionary history. The Mg^{2+}-μc's are located at functionally important regions of the ribosome, and are associated with unusual conformational states of RNA, forming intricate binding surfaces.

Mg^{2+}-μc's D1, D2 and D4 but not loop-L2/D2 are conserved in all mitoribosomes. Mitoribosomes have been substantially remodeled over time, as can be seen by comparison of extant mitoribosomes with those of the ancestral endosymbiont (51,53,54). Mitoribosomes have twice the protein and half the rRNA of the bacterial ribosome. Although rRNA secondary elements that contain Mg^{2+}-μc's D1, D2 and D4 are conserved all mitoribosomes, loop-L2/D2 appears to be absent from mitoribosomes other than those of fungi (Table 1). In the human mitoribosome protein L8 (the mammalian equivalent of L2), the N-terminus has been replaced by a sequence that diverges widely from loop-L2/D2 (Table 1). It may be that loop-L2/D2 has been structurally replaced by a nuclear encoded protein with unrelated sequence.

SUMMARY

The ribosomal peptidyl transferase center (PTC) is supported by a framework of magnesium microclusters (Mg^{2+}-μc's). Mg^{2+}-μc's are characterized by direct phosphate chelation of two magnesium ions in the form of $Mg^{2+}_{(a)}$–(O1P-P-O2P)–$Mg^{2+}_{(b)}$, phosphate groups of adjacent RNA residues as first-shell ligands of a common Mg^{2+} ion, and undulated RNA surfaces with unpaired and unstacked bases.

SUPPLEMENTARY DATA

Supplementary Data are available at NAR Online.

ACKNOWLEDGEMENTS

The authors thank Drs Roger Wartell, Steve Harvey and Nicholas Hud for helpful discussions.

FUNDING

This work was funded in part by the NASA Astrobiology Institute. Funding for open access charge: NASA Astrobiology Institute.

Conflict of interest statement. None declared.

REFERENCES

1. Basu,S., Rambo,R.P., Strauss-Soukup,J., Cate,J.H., Ferre-D'Amare,A.R., Strobel,S.A. and Doudna,J.A. (1998) A specific monovalent metal ion integral to the AA platform of the RNA tetraloop receptor. *Nat. Struct. Biol.*, **5**, 986–992.
2. Cate,J.H., Hanna,R.L. and Doudna,J.A. (1997) A magnesium ion core at the heart of a ribozyme domain. *Nat. Struct. Biol.*, **4**, 553–558.
3. Cate,J.H., Gooding,A.R., Podell,E., Zhou,K., Golden,B.L., Kundrot,C.E., Cech,T.R. and Doudna,J.A. (1996) Crystal structure of a group I ribozyme domain: principles of RNA packing. *Science*, **273**, 1678–1685.
4. Cate,J.H., Gooding,A.R., Podell,E., Zhou,K., Golden,B.L., Szewczak,A.A., Kundrot,C.E., Cech,T.R. and Doudna,J.A. (1996) RNA tertiary structure mediation by adenosine platforms. *Science*, **273**, 1696–1699.
5. Juneau,K., Podell,E., Harrington,D.J. and Cech,T.R. (2001) Structural basis of the enhanced stability of a mutant ribozyme domain and a detailed view of RNA–solvent interactions. *Structure*, **9**, 221–231.
6. Cate,J.H., Yusupov,M.M., Yusupova,G.Z., Earnest,T.N. and Noller,H.F. (1999) X-ray crystal structures of 70S ribosome functional complexes. *Science*, **285**, 2095–2104.
7. Ban,N., Nissen,P., Hansen,J., Moore,P.B. and Steitz,T.A. (2000) The complete atomic structure of the large ribosomal subunit at 2.4 Å resolution. *Science*, **289**, 905–920.
8. Wimberly,B.T., Brodersen,D.E., Clemons,W.M. Jr., Morgan-Warren,R.J., Carter,A.P., Vonrhein,C., Hartsch,T. and Ramakrishnan,V. (2000) Structure of the 30S ribosomal subunit. *Nature*, **407**, 327–339.
9. Harms,J., Schluenzen,F., Zarivach,R., Bashan,A., Gat,S., Agmon,I., Bartels,H., Franceschi,F. and Yonath,A. (2001) High resolution structure of the large ribosomal subunit from a mesophilic eubacterium. *Cell*, **107**, 679–688.
10. Yusupov,M.M., Yusupova,G.Z., Baucom,A., Lieberman,K., Earnest,T.N., Cate,J.H. and Noller,H.F. (2001) Crystal structure of the ribosome at 5.5 A resolution. *Science*, **292**, 883–896.
11. Klein,D.J., Moore,P.B. and Steitz,T.A. (2004) The contribution of metal ions to the structural stability of the large ribosomal subunit. *RNA*, **10**, 1366–1379.
12. Berk,V., Zhang,W., Pai,R.D. and Cate,J.H. (2006) Structural basis for mRNA and tRNA positioning on the ribosome. *Proc. Natl Acad. Sci. USA*, **103**, 15830–15834.
13. Selmer,M., Dunham,C.M., Murphy,F.V.t., Weixlbaumer,A., Petry,S., Kelley,A.C., Weir,J.R. and Ramakrishnan,V. (2006) Structure of the 70S ribosome complexed with mRNA and tRNA. *Science*, **313**, 1935–1942.
14. Voss,N.R., Gerstein,M., Steitz,T.A. and Moore,P.B. (2006) The geometry of the ribosomal polypeptide exit tunnel. *J. Mol. Biol.*, **360**, 893–906.
15. Tinoco,I. Jr and Bustamante,C. (1999) How RNA folds. *J. Mol. Biol.*, **293**, 271–281.
16. Brion,P. and Westhof,E. (1997) Hierarchy and dynamics of RNA folding. *Annu. Rev. Biophys. Biomol. Struct.*, **26**, 113–137.
17. Westheimer,F.H. (1987) Why nature chose phosphates. *Science*, **235**, 1173–1178.
18. Hsiao,C., Tannenbaum,M., VanDeusen,H., Hershkovitz,E., Perng,G., Tannenbaum,A. and Williams,L.D. (2008) In Hud,N.

(ed.), *Nucleic Acid Metal Ion Interactions*. The Royal Society of Chemistry, London, pp. 1–35.
19. Brown,I.D. (1988) What factors determine cation coordination numbers. *Acta Crystallogr. Sect. B.*, **44**, 545–553.
20. Brown,I.D. (1992) Chemical and steric constraints in inorganic solids. *Acta Crystallogr. Sect. B.*, **48**, 553–572.
21. Bock,C.W., Katz,A.K., Markham,G.D. and Glusker,J.P. (1999) Manganese as a replacement for magnesium and zinc: functional comparison of the divalent ions. *J. Am. Chem. Soc.*, **121**, 7360–7372.
22. Rashin,A.A. and Honig,B. (1985) Reevaluation of the born model of ion hydration. *J. Phys. Chem.*, **89**, 5588–5593.
23. Berman,H.M., Westbrook,J., Feng,Z., Gilliland,G., Bhat,T.N., Weissig,H., Shindyalov,I.N. and Bourne,P.E. (2000) The protein data bank. *Nucleic Acids Res.*, **28**, 235–242.
24. Apostolico,A., Ciriello,G., Guerra,C., Heitsch,C.E., Hsiao,C. and Williams,L.D. (2009) Finding 3D motifs in ribosomal RNA structures. *Nucleic Acids Res.*, **21**, 21.
25. Richardson,J.S., Schneider,B., Murray,L.W., Kapral,G.J., Immormino,R.M., Headd,J.J., Richardson,D.C., Ham,D., Hershkovits,E., Williams,L.D. *et al.* (2008) RNA backbone: Consensus all-angle conformers and modular string nomenclature (an RNA Ontology Consortium contribution). *RNA*, **14**, 1–17.
26. Hsiao,C., Mohan,S., Hershkovitz,E., Tannenbaum,A. and Williams,L.D. (2006) Single nucleotide RNA choreography. *Nucleic Acids Res.*, **34**, 1481–1491.
27. Hershkovitz,E., Sapiro,G., Tannenbaum,A. and Williams,L.D. (2006) Statistical analysis of the RNA backbone. *IEEE/ACM Trans. Comp. Biol. Bioinformatics*, **3**, 33–46.
28. Hershkovitz,E., Tannenbaum,E., Howerton,S.B., Sheth,A., Tannenbaum,A. and Williams,L.D. (2003) Automated identification of RNA conformational motifs: theory and application to the HM LSU 23S rRNA. *Nucleic Acids Res.*, **31**, 6249–6257.
29. Stefan,L.R., Zhang,R., Levitan,A.G., Hendrix,D.K., Brenner,S.E. and Holbrook,S.R. (2006) MeRNA: a database of metal ion binding sites in RNA structures. *Nucleic Acids Res.*, **34**, D131–D134.
30. Altschul,S.F., Madden,T.L., Schaffer,A.A., Zhang,J., Zhang,Z., Miller,W. and Lipman,D.J. (1997) Gapped BLAST and PSI-BLAST: a new generation of protein database search programs. *Nucleic Acids Res.*, **25**, 3389–3402.
31. Larkin,M.A., Blackshields,G., Brown,N.P., Chenna,R., McGettigan,P.A., McWilliam,H., Valentin,F., Wallace,I.M., Wilm,A., Lopez,R. *et al.* (2007) Clustal W and Clustal X version 2.0. *Bioinformatics*, **23**, 2947–2948.
32. Hansen,J.L., Schmeing,T.M., Klein,D.J., Ippolito,J.A., Ban,N., Nissen,P., Freeborn,B., Moore,P.B. and Steitz,T.A. (2001) Progress toward an understanding of the structure and enzymatic mechanism of the large ribosomal subunit. *Cold Spring Harb. Symp. Quant. Biol.*, **66**, 33–42.
33. Toor,N., Keating,K.S., Taylor,S.D. and Pyle,A.M. (2008) Crystal structure of a self-spliced group II intron. *Science*, **320**, 77–82.
34. Noller,H.F. (2004) The driving force for molecular evolution of translation. *RNA*, **10**, 1833–1837.
35. Uhlein,M., Weglohner,W., Urlaub,H. and Wittmann-Liebold,B. (1998) Functional implications of ribosomal protein L2 in protein biosynthesis as shown by in vivo replacement studies. *Biochem. J.*, **331**, 423–430.
36. Cooperman,B.S., Wooten,T., Romero,D.P. and Traut,R.R. (1995) Histidine 229 in protein L2 is apparently essential for 50S peptidyl transferase activity. *Biochem. Cell. Biol.*, **73**, 1087–1094.
37. Diedrich,G., Spahn,C.M., Stelzl,U., Schafer,M.A., Wooten,T., Bochkariov,D.E., Cooperman,B.S., Traut,R.R. and Nierhaus,K.H. (2000) Ribosomal protein L2 is involved in the association of the ribosomal subunits, tRNA binding to A and P sites and peptidyl transfer. *EMBO J.*, **19**, 5241–5250.
38. Meskauskas,A., Russ,J.R. and Dinman,J.D. (2008) Structure/function analysis of yeast ribosomal protein L2. *Nucleic Acids Res.*, **7**, 7.
39. Nissen,P., Hansen,J., Ban,N., Moore,P.B. and Steitz,T.A. (2000) The structural basis of ribosome activity in peptide bond synthesis. *Science*, **289**, 920–930.
40. Noller,H.F., Hoffarth,V. and Zimniak,L. (1992) Unusual resistance of peptidyl transferase to protein extraction procedures. *Science*, **256**, 1416–1419.
41. Carter,A.P., Clemons,W.M., Brodersen,D.E., Morgan-Warren,R.J., Wimberly,B.T. and Ramakrishnan,V. (2000) Functional insights from the structure of the 30S ribosomal subunit and its interactions with antibiotics. *Nature*, **407**, 340–348.
42. Robertson,M.P., Igel,H., Baertsch,R., Haussler,D., Ares,M. Jr and Scott,W.G. (2005) The structure of a rigorously conserved RNA element within the SARS virus genome. *PLoS Biol.*, **3**, e5.
43. Beese,L.S. and Steitz,T.A. (1991) Structural basis for the 3′-5′ exonuclease activity of Escherichia coli DNA polymerase I: a two metal ion mechanism. *EMBO J.*, **10**, 25–33.
44. Steitz,T.A. and Steitz,J.A. (1993) A general two-metal-ion mechanism for catalytic RNA. *Proc. Natl Acad. Sci. USA*, **90**, 6498–6502.
45. Martins,E.P. and Hansen,T.F. (1997) Phylogenies and the comparative method: a general approach to incorporating phylogenetic information into the analysis of interspecific data. *Am. Nat.*, **149**, 646–667.
46. Rost,B. (1999) Twilight zone of protein sequence alignments. *Protein Eng.*, **12**, 85–94.
47. Heinz,D.W., Baase,W.A., Zhang,X.J., Blaber,M., Dahlquist,F.W. and Matthews,B.W. (1994) Accommodation of amino acid insertions in an alpha-helix of T4 lysozyme. Structural and thermodynamic analysis. *J. Mol. Biol.*, **236**, 869–886.
48. Olsen,G.J. and Woese,C.R. (1997) Archaeal genomics: an overview. *Cell*, **89**, 991–994.
49. Cannone,J.J., Subramanian,S., Schnare,M.N., Collett,J.R., D'Souza,L.M., Du,Y., Feng,B., Lin,N., Madabusi,L.V., Muller,K.M. *et al.* (2002) The comparative RNA web (CRW) site: an online database of comparative sequence and structure information for ribosomal, intron, and other RNAs. *BMC Bioinformatics*, **3**, 2.
50. Mears,J.A., Sharma,M.R., Gutell,R.R., McCook,A.S., Richardson,P.E., Caulfield,T.R., Agrawal,R.K. and Harvey,S.C. (2006) A structural model for the large subunit of the mammalian mitochondrial ribosome. *J. Mol. Biol.*, **358**, 193–212.
51. Sharma,M.R., Koc,E.C., Datta,P.P., Booth,T.M., Spremulli,L.L. and Agrawal,R.K. (2003) Structure of the mammalian mitochondrial ribosome reveals an expanded functional role for its component proteins. *Cell*, **115**, 97–108.
52. Mears,J.A., Cannone,J.J., Stagg,S.M., Gutell,R.R., Agrawal,R.K. and Harvey,S.C. (2002) Modeling a minimal ribosome based on comparative sequence analysis. *J. Mol. Biol.*, **321**, 215–234.
53. Smits,P., Smeitink,J.A., van den Heuvel,L.P., Huynen,M.A. and Ettema,T.J. (2007) Reconstructing the evolution of the mitochondrial ribosomal proteome. *Nucleic Acids Res.*, **35**, 4686–4703.
54. O'Brien,T.W. (2003) Properties of human mitochondrial ribosomes. *IUBMB Life*, **55**, 505–513.